ISBN: 978-1-925627-03-9

Convergence of the 2D Free-Surface Flow Equations (or SWE) using a Parallelised Finite Volume Solution

Greg Collecutt[1], Bill Syme[2]

[1]Principal Engineer, BMT WBM, Brisbane, Australia
E-mail: greg.collecutt@bmtwbm.com.au

[2]Senior Principal, BMT WBM, Brisbane, Australia

Two-dimensional (2D) solutions of free-surface flow of long waves (e.g. floods and tides) typically use the Shallow Water Equations (SWE) as the governing equations. However, the equations are often simplified by removal of terms, and/or through using lower order temporal and spatial solutions. The effect of these simplifications is often not fully understood by modellers, resulting in (often oblivious) loss of accuracy and inappropriate application.

Efforts have been made in recent times to better understand differences between 2D solutions, with the most notable being the UK Environment Agency's 2D benchmarking studies. However, the authors observed that whilst these benchmarking studies assist in understanding the performance of 2D solvers, there are more challenging situations that the current benchmarking suite does not cover, such as flows around sharp bends. During the development of the new TUFLOW HPC 2nd order spatial FV 2D SWE solver for application on parallelised hardware architecture, interesting observations were encountered whilst testing for solution convergence at the flume and real-world scale. The new scheme and convergence observations are discussed and presented.

1. INTRODUCTION

Nearly every real world application for flood modelling involves estimating head losses in areas of changing velocity. Such changes may occur due to changing direction of the flow path and/or changes in cross-sectional area of the channel due to width or depth variation. The ability of any numerical scheme to accurately compute the head (energy) losses associated with such changes depends on the mathematics of the scheme, the resolution the geometry is modelled, the choice of eddy viscosity model, and possibly the size of the time step used for transient solutions.

Results from any model with spatial discretisation, ideally, should converge asymptotically to limiting values as the spatial resolution is increased (i.e. element size reduced). However, this can be more difficult to realise in practice than might be thought for a couple of reasons: increasing model resolution may admit new flow details to the solution that are real and expected; and numerical rounding errors may accumulate leading to artefact divergence in the results at very fine mesh resolutions (particularly for matrix solvers). These difficulties should not deter a modeller from performing mesh-size sensitivity studies, as there are at least three strong arguments for performing such investigations.

Firstly, unacceptably changing results with mesh size may well indicate a flawed solution scheme, incorrect computer code, or poorly defined model boundary conditions (such as point sources or

sinks). Mesh-size sensitivity studies should be performed if for no other reason than to build confidence in both the model and the software.

Secondly, mesh-size sensitivity studies may aid in the calibration process, in that some discrepancy between model results and calibration data may be understood and hence tolerated if it can be shown that the results are converging towards the calibration data as the mesh size is refined.

Thirdly, the mesh-size sensitivity study also helps understand mesh size contribution to uncertainty in key model results, and should perhaps be added to the variations identified by other sensitivity studies such as variation in bed-friction coefficients and/or inflows.

In the process of developing the new TUFLOW HPC solver, Collecutt & Syme (2017), its mesh size convergence for applications were investigated, two of which are presented here. The first application is a laboratory scale flume test in which water flows around a right angled bend in a rectangular section channel. Test data exists for this case making it particularly valuable. The second test case utilises a well calibrated real river model with significant sinuosity and depth variation.

Both the original TUFLOW ADI scheme, Syme (1991), and the HPC solver incorporate a Smagorinsky eddy viscosity model. This model uses two terms, one of which is a function of cell area. During the investigations, it became apparent that this term was changing in magnitude with mesh size, and that this was contributing to mesh size dependence in the results. This is discussed in detail within.

2. TUFLOW HPC

The TUFLOW HPC solver resolves the 2D Shallow Water Equations (SWE) on a uniform Cartesian grid using finite volume schemes (Collecutt and Syme, 2017). Water depth, h, and the u and v velocity, utilise offset grids as shown in Figure 1. The solid black circles represent the points at which the cell averaged depth, h, is defined. The u velocities, are defined at the horizontal mid-points, shown with red crosses, and the v velocities, are defined at the vertical mid-points, shown with green plus symbols.

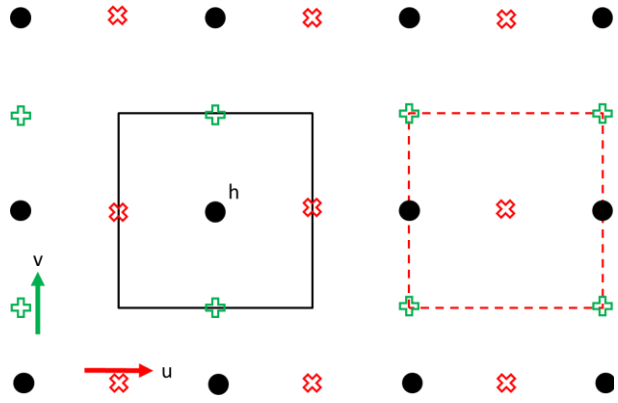

Figure 1 Offset Grid

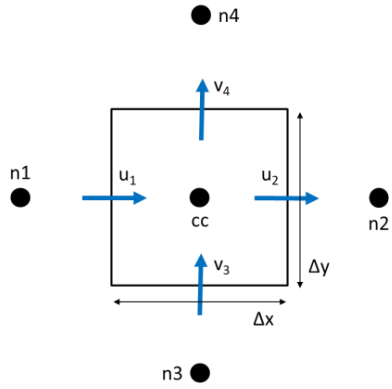

Figure 2 Finite Volume Scheme

The time rate of change of the cell averaged water depth (or volume) is calculated with a finite volume scheme based on the black cell boundary shown in Figure 1. Similarly, the time rate of change for the u velocity (or u momentum) is calculated with a finite volume scheme based on the red dash cell boundary centred on a u velocity point (red cross symbol). The cell boundary for the v velocity (or v momentum) is not shown, but would centre on a v velocity point (green plus symbol). Depth and u and v velocities are propagated forward in time using the classic fourth order Runge-Kutta method based on four time derivate evaluations per time step.

The finite volume scheme for calculating the rate of change of cell depth is illustrated in Figure 2. The cell centre (for the cell in question) is given the notation cc, while the surrounding neighbours are given the notation n1..n4. The u velocity at the left and right faces are notated u1 and u2, and the v velocities at the bottom and top faces are notated v3 and v4. The cell width and height are Δx and Δy respectively. The time rate of change for the cell averaged depth is shown in Equation 1.

$$\frac{A\partial h}{\partial t} = \Phi_1 - \Phi_2 + \Phi_3 - \Phi_4 + S_Q \quad (1)$$

Where the Φ_i are the volume fluxes through the four faces, and S_Q is the net volume source from rain, pipes, soil infiltration, and any flow linkages to 1D elements. By computing the face fluxes for all model faces, and then referencing these when computing the depth derivative for each cell, volume conservation is guaranteed to numerical precision.

The calculation of the face volume fluxes is central to the operation of the solver. The basic form of this calculation for right and top faces is shown in Equation 2, where u_2 and v_4 are already defined at the cell mid-sides. The critical problem is the computation of water depth at the cell boundaries. For the first order scheme, this is depth of the *upstream* cell, bounded to be greater than or equal to 0, and less than or equal to the surface elevation of the upstream cell less the bed elevation at the cell side mid-point in question. The face fluxes may also be factored down by flow constriction factors where sub-grid-scale interfering geometries exist.

$$\Phi_2 = \Delta y h_{f2} u_2 \qquad \Phi_4 = \Delta x h_{f4} v_4 \quad (2)$$

For the second order spatial scheme the depth at the face is computed as the average of the two cell averaged depths, however this method in its simplest form is not total variation diminishing (TVD) and is known to be unstable. A hybrid method is implemented in which the depth at the cell face transitions from interpolated depth, in the limit of a smoothing varying solution, to the upstream depth when the solution shows short scale reversal.

The finite volume schemes for calculating the velocity time derivatives are the same in principle, but considerably more complex due to the offset grid. To detail them here is beyond the intent of this paper. However, it is important to define the Smagorinsky eddy viscosity model, as shown in Equation 3.

$$\nu_T = mA\left[\left(\frac{\partial u}{\partial x}\right)^2 + \left(\frac{\partial v}{\partial y}\right)^2 + \frac{1}{2}\left(\frac{\partial u}{\partial y} + \frac{\partial v}{\partial x}\right)^2\right]^{\frac{1}{2}} + c \quad (3)$$

The kinematic turbulent viscosity, ν_T, is computed as a linear function of the magnitude of the velocity gradient tensor with proportional term mA (where A is the cell area) and constant offset c. It is essential to understand how this model changes with mesh resolution. Where velocity gradients are inversely proportional to mesh size (for example flow around a sharp corner) the proportional term of Equation 3 becomes proportional to cell spacing. When velocity gradients are not related to mesh size (e.g. in the middle of open water), the proportional term becomes proportional to cell spacing squared. In both cases, the proportional terms diminish to zero in the limit of infinite mesh resolution, and only the constant term, c, remains.

The calculation steps detailed above are highly independent. The calculation of flux for one face may be performed independently of the other faces, and likewise the summation of flux for each cell volume may be performed independently of the other cell volumes. Applying the same algorithm to millions of data elements is ideally suited to modern multi-core CPUs and particularly suited to GPU hardware acceleration.

3. RIGHT ANGLED FLUME

The first benchmark test considered is that of sub-critical flow around an abrupt 90 degree angled bend, as performed by Malone and Parr (2008). Their test setup consisted of two flat bottomed flumes connected at an angle, with the downstream depth and the volume flow rate able to be varied. Malone and Parr measured the head loss attributable to the bend over a range of flow rates, water depths, bend angles, and performed a detailed analysis. The flow regimes (downstream water depth vs volume flow rate) tested are shown in Figure 3 along with a linear fit for head loss as a function of velocity head. The slope of this linear fit is the head loss factor, which represents the ratio of total energy loss around the bend to upstream kinetic energy. For the 90 degree abrupt bend, a loss factor of 1.23 is obtained. For the majority of the tests performed, the water depths within the flumes were comparable to the flume width. This casts some doubt on the validity of modelling these tests with the SWE, but as will be shown the results agree surprisingly well.

Here only the 90 degree abrupt bend is considered, with flow rate 0.008 m^3/s, and downstream water level 0.123 m. The flume width was 0.15 m, and the upstream and downstream arms were 18 widths long. The bed friction (Manning's) coefficient was set to 0.01, and both arms had a downhill gradient of 0.2%. The numerical solution is also expected to depend on mesh size, viscosity coefficients, spatial interpolation scheme, and time step. Figure 4 illustrates the flow solutions at the bend for mesh sizes ranging from 2, 4, 8 and 16 cells across the flume width resulting in mesh cell sizes less than 1 cm. Flow enters from left and exits from the bottom. The solution was found to reach a steady state by approximately 60 s from model start. Each flume arm was divided into tiles of one flume width square, and the total head in each tile was spatially and temporally averaged over 1 s intervals from 60 s to 120 s. The total head in each tile was plotted as a function of distance from the bend, and a linear fit derived. The head loss attributable to the bend was calculated by extrapolating the upstream and downstream linear fits to the bend, and computing the difference.

Figure 6 plots the loss factor attributable to the bend as a function of mesh size, for the 1st and 2nd order spatial schemes and for constant viscosity values (i.e. *c* of Equation 3, in units m^2/s) and for proportional viscosity values (i.e. *m* of Equation 3, dimensionless). From these results, it can be seen that both 1st and 2nd order schemes tend to over-predict the head loss, and that both 1st and 2nd order schemes with non-zero constant viscosity asymptote to limiting values with decreasing cell size.

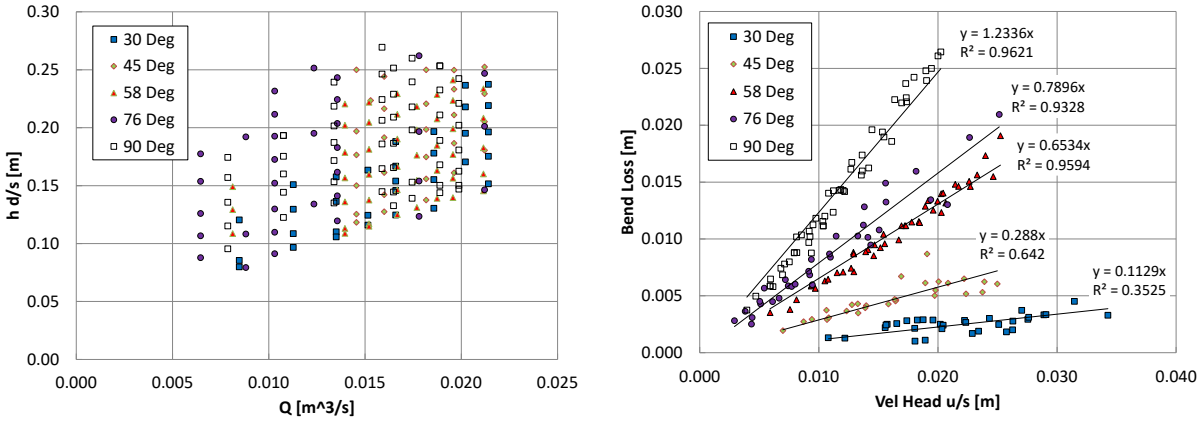

(a) Flow regimes (b) Head losses

Figure 3 Abrupt Angled Bend Test, reproduced from Malone & Parr (2008)

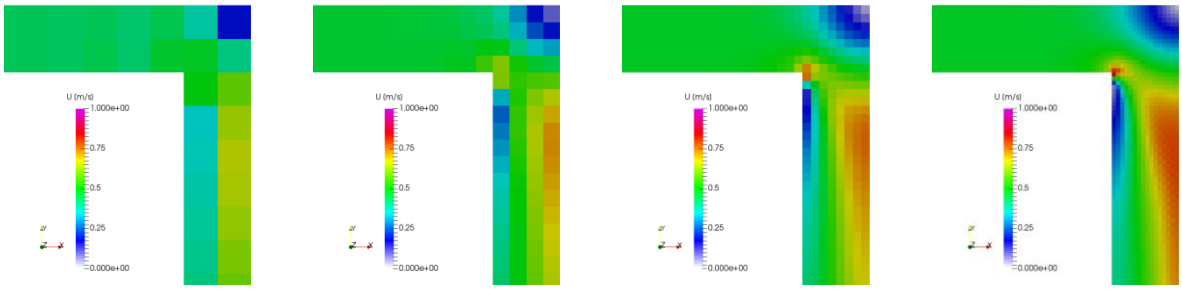

(a) N Width = 2 (b) N Width = 4 (c) N Width = 8 (d) N Width = 16

Figure 4 90 Degree Bend Flow Solutions at Various Mesh Resolutions

For both 1st and 2nd order schemes, the zero-viscosity case does not show convergence. A possible reason for this becomes apparent when a zero viscosity flow solution for a finer mesh size (in this case N Width = 23) is visualised, as shown in Figure 5, in which unrealistic, chaotic eddy structures occur. The introduction of some eddy viscosity weakens the formation of these structures. Interestingly for both 1st and 2nd order schemes, non-convergence is apparent for the various proportional (only) viscosity values trialled. The explanation for this behaviour is that, as the proportional viscosity term is

also proportional to cell area, reducing cell size leads to zero viscosity in its limit. Not only is the proportional term a source of mesh size dependence in the results, but if it is the principle contributor to viscosity within a model then the model may behave unexpectedly, even becoming unstable, as mesh size is reduced.

In summary, it appears that excellent solutions are obtained with both 1st and 2nd order spatial schemes with just enough constant viscosity to prevent chaotic eddy structures. Reasonable solutions are found utilising 3 or more cells across the flume width. At lower resolutions, the 2nd order solution shows lower head losses (and closer to the test results) than the 1st order solution.

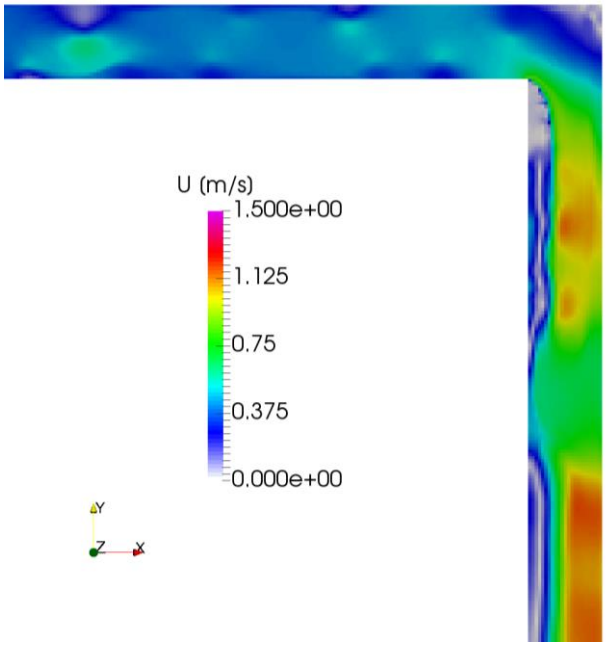

Figure 5 Chaotic Eddy Structures 2nd Order Zero Viscosity

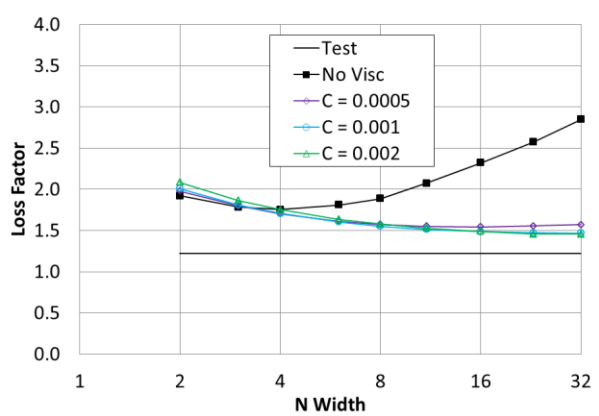

(a) 1st Order, constant viscosity values

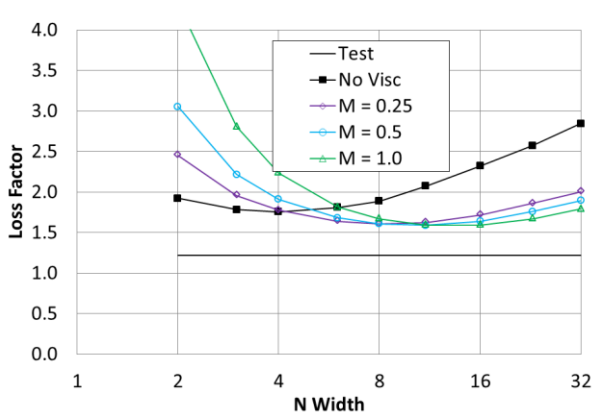

(b) 1st Order, proportional viscosity values

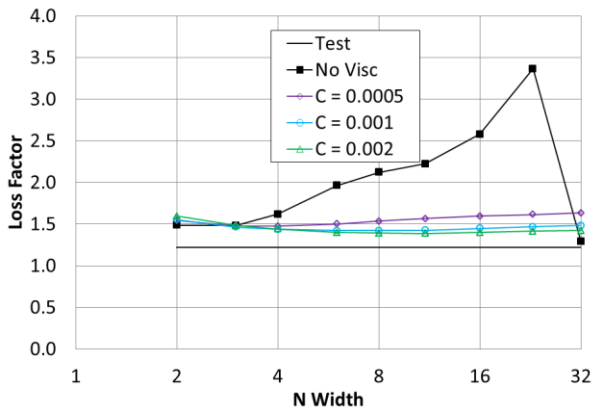

(c) 2nd Order, constant viscosity values

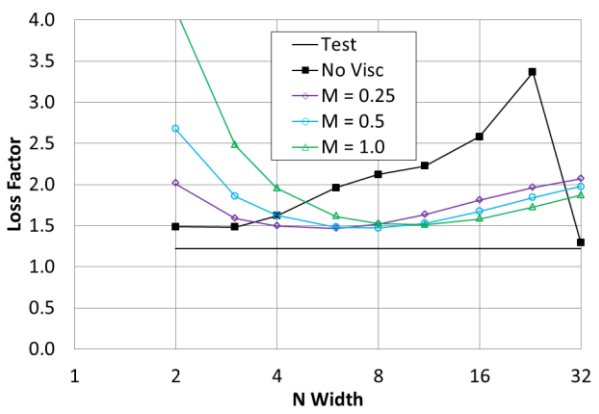

(d) 2nd Order, proportional viscosity values

Figure 6 TUFLOW HPC Abrupt 90 Degree Bend Head Loss Factor

4. REAL RIVER

The second test case utilised the bed elevation model from a calibrated, real river model as shown in Figure 7. The model is of the Brisbane River, sectioned out from the larger model used for the Brisbane River Catchment Flood Study, BMT WBM (2015). The maximum water depth (red in Figure 7) was approximately 30 m. The river is highly sinuous with rock ledges, banks and deep pools. The downstream boundary (top right of Figure 7) was held at a constant elevation of 2.7 m Australian Height Datum, and a constant inflow of 9,000 m^3/s applied at the upstream boundary. Calibrated form losses at sharp bends and bridges were removed to simplify the analysis and comparison.

The overall head loss for the river segment, shown in Figure 8, was calculated using the standard TUFLOW ADI scheme (legend CLA), and for the HPC scheme with 1st and 2nd order spatial interpolation. Cell sizes of 5, 7, 10, 15, 20, 30, and 50 m were studied. The typical river width was 200 m. Note that this condition represented a major flood state with significant depth averaged flow velocities in the order of 3 to 4 m/s, and a head loss of around 3.2 m (over approximately 11 km of river) for this flow that is consistent with known calibration data points taking into account the removal of bridges and calibrated form losses (which contribute around 20% additional head loss).

The head losses as a function of mesh size are shown in Figure 8 using TUFLOW's default Smagorinsky viscosity coefficients of m=0.5 and c=0.05 m^2/s, and for constant only viscosity of 1.0 m^2/s. Both the ADI scheme and the HPC 1st and 2nd order schemes demonstrate mesh size convergence, for both sets of viscosity coefficients. It is also apparent that the additional head losses induced with low mesh resolution are less when the constant only viscosity is used.

The additional head losses (induced with low mesh resolution) are significant in that surface elevations increase by as much as 50% of mesh converged head loss (2 meters in this case). This highlights the very real need to calibrate a model at given mesh size resolution, and to understand that changes in mesh size resolution can have a material impact on model calibration.

On the matter of calibration, if the model predicted head loss is greater than known calibration data the modeller is faced with either reducing the bed friction coefficient below industry standard values or adding negative energy (form) loss coefficients. Neither of these methods are considered industry best practice, and indicates an issue with the numerical solution. On the other hand, if the predicted head loss is less than known calibration data, calibration may be achieved by adding normal (positive) energy loss coefficients. Typically, these additional loss coefficients are accounting for losses not captured by the 2D scheme, such as fine-scale, sub-grid, obstructions and 3D effects such as helicoidal flow around a bend. This favours the selection of the 2nd order HPC scheme over the simpler 1st order solution due to its lower (and more quickly convergent) head loss predictions.

One final consideration is that, even though the head loss converges to an asymptotic limit at fine mesh resolution, this value is almost certainly not correct for the flow rate in question, and even if it was it may not be correct for other flow rates. This is because the turbulent eddy viscosity within the river is not uniform and will change with flow rate – neither the constant or Smagorinsky (which becomes constant viscosity in the limit of infinite mesh resolution) viscosity models reflect this behaviour.

Three dimensional CFD models typically utilise two equation turbulence models such as the k-epsilon and k-omega, and there are other more elaborate models published. Adapting one or more of these models to the SWE may yield head loss predictions that have less dependence on mesh size and calibrate well to a range of flow events without having to make large, and possibly inappropriate, adjustments to calibration parameters such as Manning's n values.

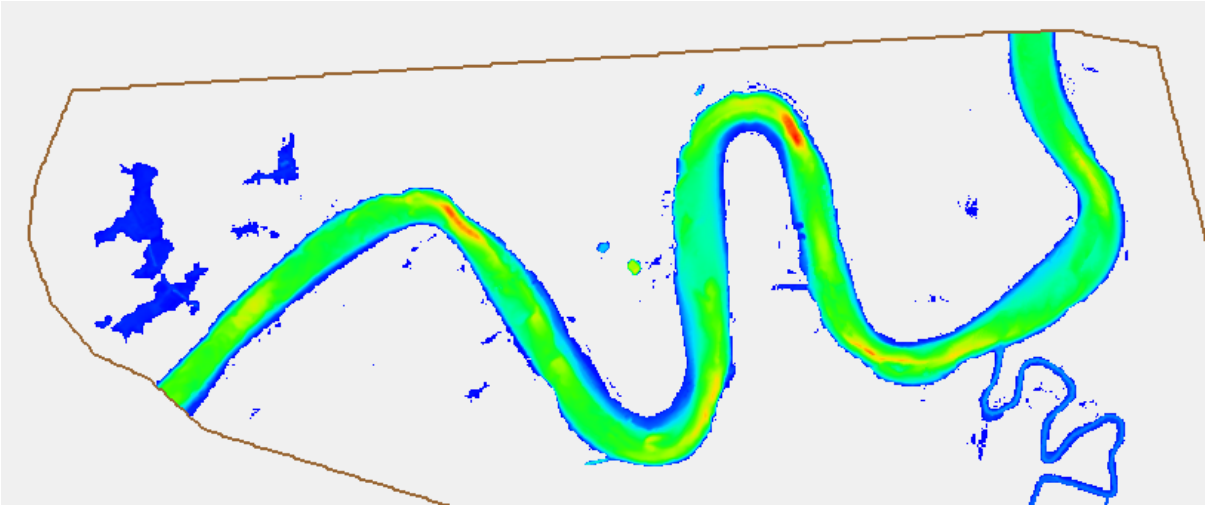

Figure 7 Real River Model, Water Depth.

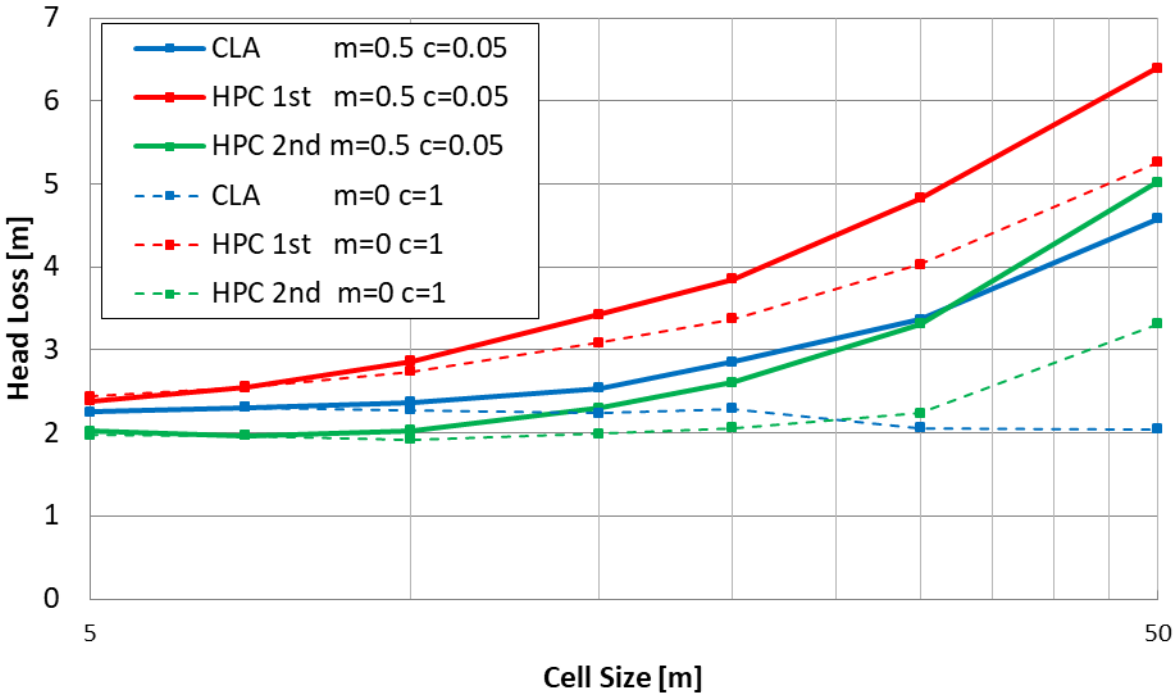

Figure 8 Real River Head Losses

5. SUMMARY

- Using the new TUFLOW HPC SWE flow solver, head loss vs mesh size investigations were performed for two flow geometries with various choices for model viscosity.
- In the case of the right angled bend in a laboratory scale rectangular section flume, head loss predictions were shown to be asymptotically convergent only in the case of non-zero constant viscosity.
- The proportional viscosity term in the Smagorinsky viscosity model was shown to diminish to zero in the limit of infinite mesh resolution, and in the case of zero viscosity, model solutions were found to demonstrate chaotic turbulent flow with sufficient mesh resolution, particularly with the 2nd order solver.
- With sufficient constant viscosity to prevent chaotic turbulent flow, the 2nd order spatial interpolation was found to yield better (and reasonable) comparison with test data and more rapid convergence with mesh size than the 1st order interpolation.
- Both the current TUFLOW ADI scheme and the HPC 1st and 2nd order FV TVD schemes were investigated for head loss vs mesh size for a real sinuous river channel with significant depth variation using a well calibrated model.
- For the real river model, mesh size convergence was demonstrated for the TUFLOW default Smagorinsky viscosity coefficients and also for constant viscosity only. In all cases bar one the predicted head losses increased with mesh size – the exception was for the ADI scheme with constant only viscosity, which showed little dependency on mesh size.
- The proportional Smagorinsky term, for both the ADI scheme and the HPC schemes, was shown to contribute to mesh size sensitivity in the results.
- These results serve as a reminder of the need for model calibration where possible, and to remind the modeller that changes in mesh size may have a material effect on results.
- Further research into the utility of more advanced eddy viscosity models for the SWEs is recommended.

6. REFERENCES

Collecutt, G. Syme, W. J. (2017). Experimental Benchmarking of Mesh Size and Time Step Convergence for a 1st and 2nd Order SWE Finite Volume Scheme. Proceedings of the 37th IAHR World Congress August 13 – 18, 2017, Kuala Lumpur, Malaysia.

Syme, W.J. (1991*). Dynamically Linked Two-Dimensional / One-Dimensional Hydrodynamic Modelling Program for Rivers, Estuaries & Coastal Waters*. PhD Thesis, Dept. of Civil Engineering, The University of Queensland, May 1991

Malone, T and Parr, D. (2008). *Bend Losses in Rectangular Culverts*, Kansas Department of Transport (http://ntl.bts.gov/lib/30000/30900/30935/KU-05-5_Final_Report.pdf)

BMT WBM (2015), BRCFS Hydraulic Assessment Technical Reports – Hydraulic Milestone Report 3: Detailed Model Development and Calibration, Draft Final, September 2015 (https://publications.qld.gov.au/dataset/brisbane-river-catchment-flood-study).